THE EFFECT OF WELD HEAT-AFFECTED ZONE HOT CRACKS ON THE FATIGUE CRACK GROWTH BEHAVIOR OF AS-CAST ALLOY 718

E. L. Bradley, III* and R. G. Thompson

Department of Materials Engineering
University of Alabama at Birmingham
Birmingham, AL 35294

Abstract

The fatigue crack propagation (FCP) behavior of weld heat-affected zone (HAZ) hot cracks in nickel cast alloy 718 was compared to that of typical fatigue cracks in the as-cast alloy. FCP rates for both types of cracks were essentially the same. Fractographic examination of the fatigue surfaces supported the data. Optical microscopic examination parallel to the fracture surface revealed that both types of fatigue cracks grew normal to the growth direction of the dendrite arms. This resulted from the orientation of the primary slip planes of the dendrites in the cast structure coinciding with the plane strain constraints at the fatigue crack tip.

Introduction

Alloy 718, in both cast and wrought forms, is widely used in industry due to its excellent weldability. However, 718 can be susceptible to hot cracking during welding when sufficient restraint and thermal stresses are present in the heat-affected zone (HAZ) of the welds. These cracks form from the presence of liquid at the grain boundaries in the HAZ (1) and this liquid is believed to develop from liquation of the Laves and NbC in the interdendritic region. (2) Figure 1 shows a typical as-cast microstructure where the darkened areas are the heavily segregated interdendritic region which contains Laves phase, niobium carbide (NbC), and orthorhombic Ni_3Nb (δ) phase. Laves, which has a lower melting temperature than the surrounding matrix (3), melts in the HAZ and mixes with liquid from the constitutional liquation of the NbC. (4) The build up of strain caused by restraint and thermal stresses in the welded part cause the grain boundaries with this liquid present to open as cracks. The crack which forms lies in the interdendritic region and along the interdendritic phases which produced the liquid during welding that allowed the hot crack to form. Thus, the hot crack has a special microstructural starting geometry that begins in the interdendritic region and lies at a grain boundary. It was hypothesized that due to this unique geometry the hot crack might exhibit anomalous behavior during the early stages of crack growth.

Our experimental program was designed to develop an FCP data base and characterize the mechanism of fatigue crack propagation in the as-cast alloy 718. Although the fatigue crack propagation behavior of the wrought alloy 718 is well documented, (5,6,7,8) the cast alloy has received no treatment in the open literature. A further objective of this research was to compare the fatigue crack propagation behavior of samples containing hot cracks to this standard and

*Now with the Department of Materials Science and Mineral Engineering, University of California, Berkeley and Center for Advanced Materials, Lawrence Berkeley Laboratory, Berkeley, CA 94720

Superalloy 718—Metallurgy and Applications
Edited by E.A. Loria
The Minerals, Metals & Materials Society, 1989

determine what differences may exist and to determine their causes. It is hoped that the results will provide a more accurate way to incorporate the effect of hot cracks on the fatigue life of welded nickel-base superalloys.

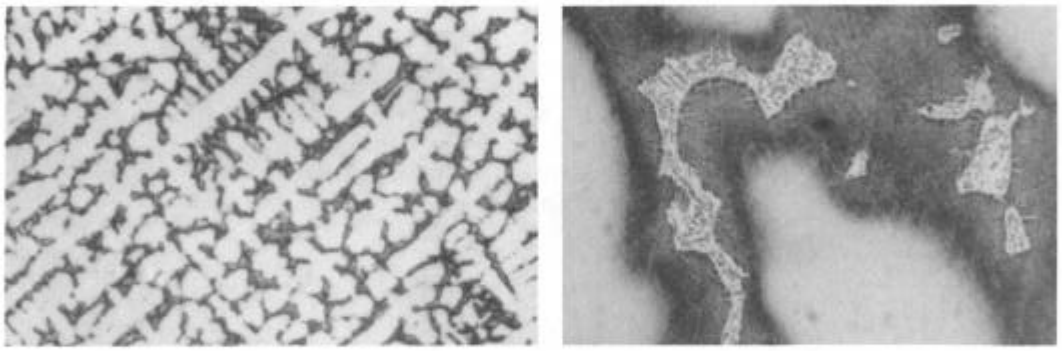

Figure 1 - Microstructure of as-cast alloy 718 at a) low and b) high magnification.

Experimental Procedure

The as-cast nickel alloy 718 used for this research was obtained from the Rocketdyne Division of Rockwell International and was prepared by vacuum induction remelting. The alloy was received in the as-cast condition as machined blanks of 109.2 x 63.5 x 3.2 mm (4.3 x 2.5 x 0.125 in) and within composition specifications. A typical heat is shown in Table I.

Table I. Composition of the As-Cast Alloy 718

Ni 53.77	Mo 3.15	Cu 0.01	B 0.002
Cr 20.46	Ti 1.09	Co 0.01	C 0.023
Fe Balance	Al 0.53	Si 0.01	S 0.004
	Nb+Ta 4.39	Mn 0.01	

Tensile tests were performed on two small, rectangular billets of dimensions 63.5 x 19.1 x 3.2 mm (2.5 x 0.75 x 0.125 in.). The samples were pulled in a servo-hydraulic unit and did not conform to the guidelines of ASTM E8 due to a lack of material.

The fatigue tests were carried out under the guidelines of ASTM E647 except for the notch preparation in the control samples as described below. Two different specimen geometries were employed. The compact tension (CT) geometry (Figure 3a) was used for the preliminary fatigue characterization and development of a data base for as-cast 718 fatigue crack growth. A modified center-cracked tension (MCCT) specimen geometry (Figure 3b) was used for the study of the fatigue response of hot cracks.

The test conditions for all samples are shown in Table II. All tests were conducted at room temperature with a loading frequency of 30Hz. An R-ratio (K_{min}/K_{max}) of 0.5 was chosen for all samples since there appeared to be some crack closure at a preliminary test done a R = 0.1.

There was no evidence of crack closure for the tests performed at R = 0.5 as the crack tips appeared to open below the minimum load applied in the fatigue tests when observed through the microscope. The samples were were initially loaded at low ΔK values which were increased until crack growth was measured.

The crack length measurements were performed using a microscope with a filar eyepiece which allowed the crack growth increment (da) to be measured within 3% of the actual value. The surfaces of the sample were mechanically polished to 0.05 μm to make the crack tip more visible in the and the samples were ultrasonically cleaned in acetone before testing.

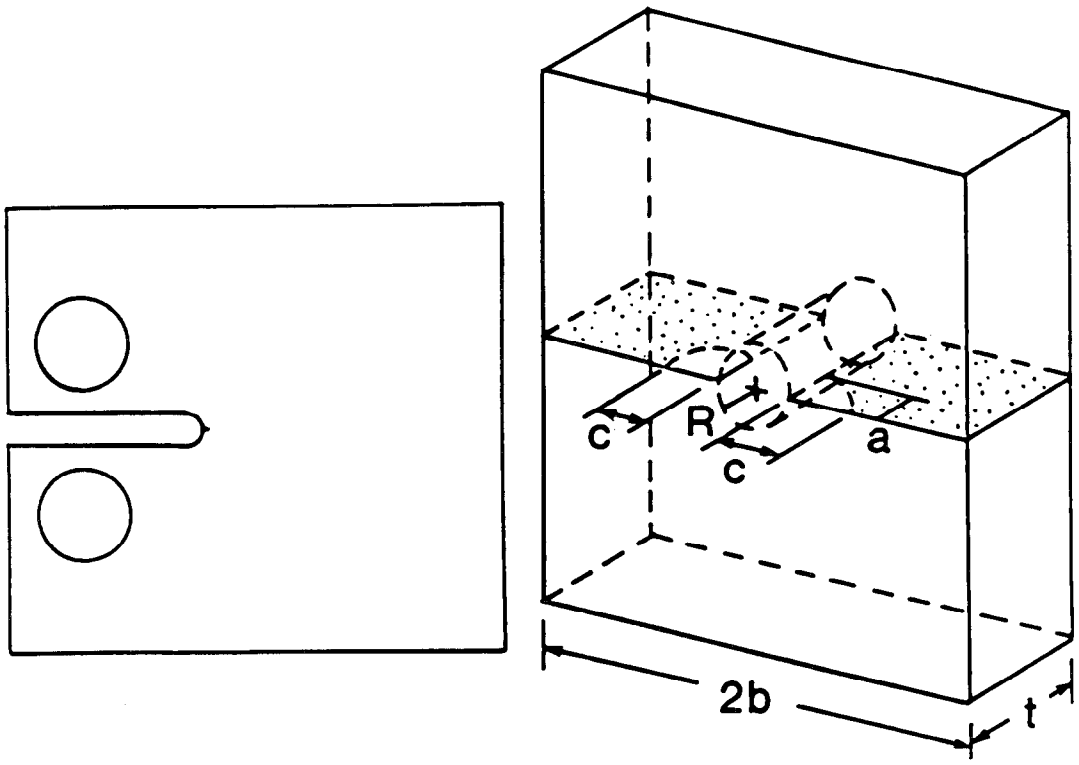

a) b)

Figure 3 - Schematics of a) CT and b) MCCT samples.

Table II. Test Conditions for Samples

Sample	Geometry	Type	Condition
3	CT	Control	As-Cast
5	CT	Control	As-Cast
6	CT	Control	As-Cast
9	MCCT	Hot Cracked	As-Cast
10L	MCCT	Hot Cracked	As-Cast
10R	MCCT	Hot Cracked	As-Cast
17	MCCT	Hot Cracked	Aged

The samples to be tested with hot cracks present were machined to 109.2 x 41.9 x 3.2 mm (4.3 x 1.65 x 0.125 in) and then surface ground to remove all prior machining marks. The samples were then loaded into a varestraint machine for HAZ hot cracking. (9) The varestraint machine applies a spot weld to the sample and then applies a bending strain that simulates weld restraint. There was a precise dwell time between the weld and the strain such that the hot cracks would lie in the fusion zone and HAZ. The fusion zone was then milled out, leaving a stress relieved HAZ with the hot cracks intercepted by the through thickness hole. This resulted in the corner-crack at a hole geometry shown in Figure 3b. The varestraint process usually opens up several cracks in the weld HAZ, but only a maximum of two of the cracks (one on either side of the hole) will grow due to their preferred orientation with respect to the stress axis. After hot cracking, the samples were flattened using a servo-hydraulic testing unit. This method assured that all the samples were cold worked the same amount and minimized any residual stress in the samples during the fatigue testing.

The control samples were machined to 63.5 x 61.0 x 3.2 mm (2.5 x 2.4 x 0.125 in) and a diamond saw was used to cut a short, thin notch at the end of the blunt notch that would nucleate the starter crack at the proper point in the sample. Control sample 3 was tested in the as-received condition with no bending. However, samples 5 and 6 were tested after cold bending in the varestraint (no spot weld) and subsequent rebending back to horizontal. This allowed the effects of the cold work to be compared with the non-cold-worked sample without the additional effects of welding to influence the results.

Reflected-light microscopy (RLM) was performed on each sample to characterize the microstructures and check for any differences between the samples with respect to grain size, interdendritic spacing and inclusion content. After fatigue testing, a fracture surface from each sample was cleaned ultrasonically in acetone, and then studied in a scanning electron microscope (SEM). RLM was also performed on the mating half of the fracture surface on a profile perpendicular and adjacent to the fracture surface on all samples in order to determine if the crack followed any particular microstructural features during propagation such as grain boundaries or interdendritic regions. The samples were mounted in carbon phenolic, polished to a 0.05 μm surface finish, and etched in a 10% oxalic acid solution at 2V for approximately 5 seconds in order to preserve the edge of the fracture surface while sufficiently revealing the microstructure.

K Determination

The stress intensity factors for the hot cracked data were computed using a regression model (10) based on data from Raju and Newman (11) for dual corner cracks at a hole under remote tension. This method was chosen because of the complexity of the crack geometry and the variation in K along the crack front for various corner crack geometries.The data from Raju and Newman was generated using a 3-dimensional finite element method (FEM) to estimate K for various ratios of the corner crack dimensions a, c, R, and t (Figure 3b). The accuracy of the estimates from the model had an R-squared value of greater than 0.99 compared to the raw data.

Results

Two samples were pulled in tension to determine the yield strength of the material in the as-received condition. The values of the yield strengths were 74,000 and 73,500 psi, respectively, which corresponds to that of annealed, wrought alloy 718. (5)

FCP Data

Three control samples and four hot cracked samples (three as-cast and one fully aged) were tested to study the effect of HAZ hot cracks on the FCP behavior of as-cast alloy 718. The crack growth data is plotted as a function of the applied ΔK. The FCP data for the control samples is shown in Figure 4a and there is some scatter. The plastically deformed samples 5 and 6 had slightly higher crack growth rates than undeformed sample 3.

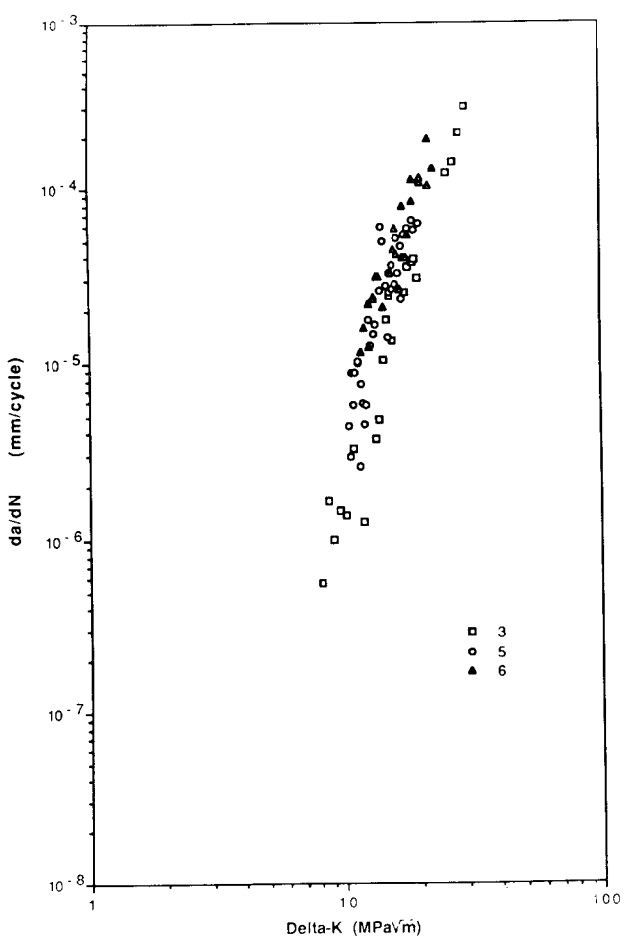

a)

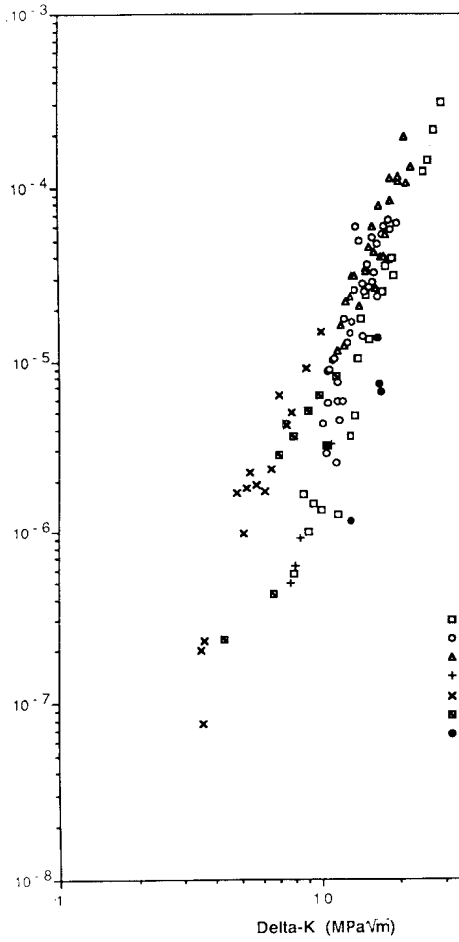

b)

Figure 4 - Crack propagation behavior of cast alloy 718 at room temperature and R = 0.5 for a) control sampl
and b) all samples together.

All FCP data for hot cracked samples were generated using a modified center-crack tension sample geometry where the hot crack made a corner-crack at a hole geometry. It can be seen in Figure 4b that the FCP data from the hot cracked samples is more scattered than that from the control samples. Sample 17, which was age-hardened, had a lower crack growth rate than those of the other samples and this agrees with the results in James and Mills study. (5) It appears that despite the scatter the FCP rates are approximately the same for the control and hot cracked samples.

The hot cracks had geometries that varied considerably and they typically were in planes at angles to that shown in Figure 3b. This was due to the orientation and position of grain boundaries which opened as cracks in the HAZ. The large grain size and the sharp thermal gradient in these samples lowered the total number of hot cracks possible in each sample. Thus the cracks that did open could vary a great deal due to these parameters. As a result only sample 10 had a crack on both sides of the hole grow measurably in fatigue.

All four hot cracked samples required a period of cyclic loading before any crack growth was measured on the front of the sample. Table III lists the initial ΔK levels the samples experienced, the number of cycles at each level, and the ΔK level at which crack growth started. This data can be explained two ways: (1) that crack nucleation was required to start the crack growing, or (2) the crack grew internally along the bore of the hole without growing at the surface due to $\Delta K_{bore} > \Delta K_{th} > \Delta K_{surface}$ along the crack front where ΔK_{th} is the threshold stress intensity. Thus the a/c ratio of the crack will change until $\Delta K_{surface} > \Delta K_{th}$. For all four samples the a/c ratios converged to unity during testing which makes this very plausible. We believe both occurred in the samples; however due to the limitations of our crack measurement equipment we could not know for certain if the crack grew along the bore of the hole without growing at the surface. Since the initial ΔK for sample 9 is greater than the ΔK at which crack growth began in sample 10 it seems certain that initiation is occurring in the samples. In addition, the low delta-K levels in sample 10 points to growth inside the sample.

As a result, the FCP results for 10L were calculated by assuming an a/c ratio (a/c= 0.700) greater than the ratio measured in the SEM for the hot crack (0.70 vs. 0.46). The ΔK value for a ratio of a/c = 0.457 results in a starting ΔK = 2.2 MPa $\sqrt{m}$ which is extremely low. The correction makes ΔK = 3.5 MPa$\sqrt{m}$.

Table III. Comparison of ΔK Levels for the Hot Cracked Samples

Sample	ΔK Level	Cycles
9	5.2	500,000
	6.3	160,000
	7.8	Crack Grew
10	2.9	720,000
	3.5	Crack Grew
17	11.1	200,000
	12.2	207,000
	13.3	Crack Grew

Fractography

The fracture surfaces of both the control and hot cracked samples were observed in the SEM to determine if any differences in crack growth mechanisms existed. A region of low ΔK crack growth in control sample 6 is shown (Figure 5a) and a faceted, crystallographic fracture surface characteristic of transgranular cleavage crack propagation is observed. Note there are

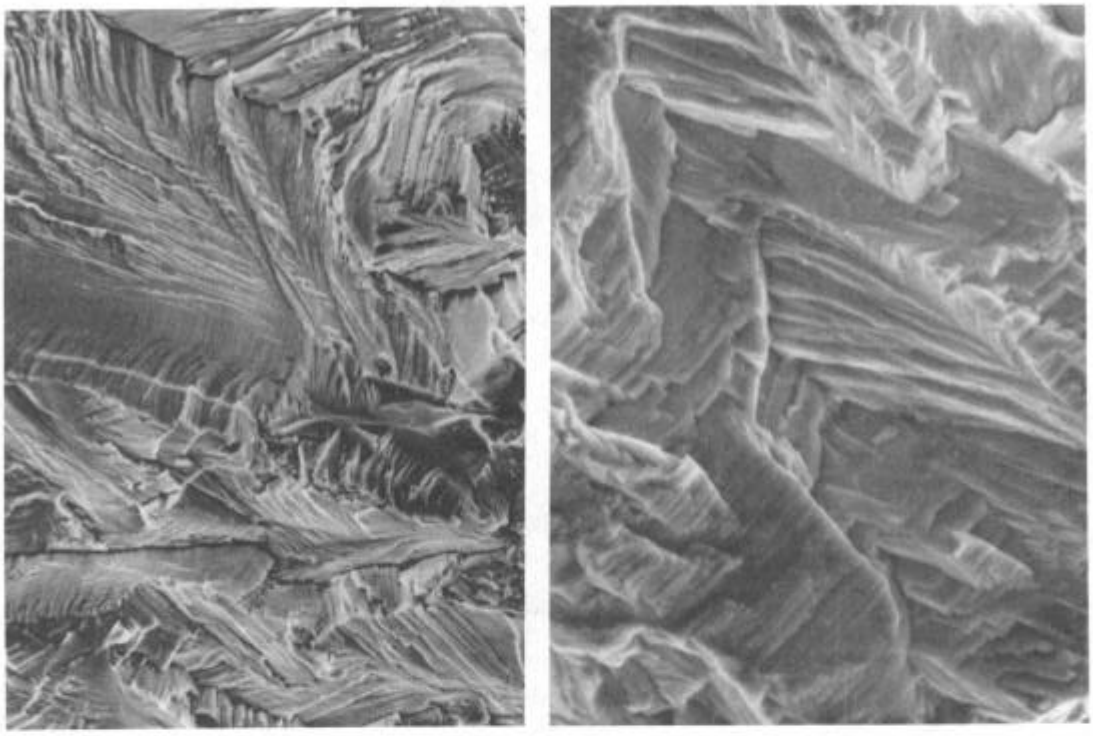

Figure 5 - Scanning electron micrographs of low ΔK crack growth in cast alloy 718 for a) control sample, and b) hot cracked sample.

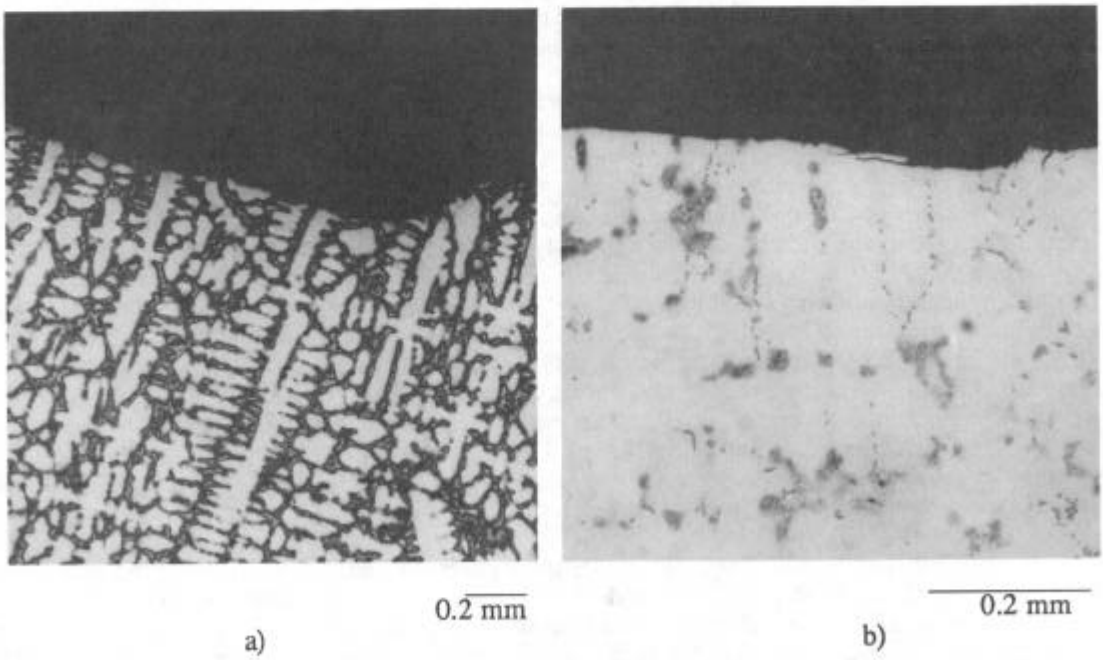

Figure 6 - Crack path morphology of the cast alloy 718 for a) control sample, and b) hot cracked sample. The profiles were taken perpendicular to the crack surface.

no ductile features on the surface that might be expected from the hard, interdendritic phases present in the material. Figure 5b is from the low ΔK crack growth region in a hot cracked sample and the surface morphology is very similar to that seen in the control samples. The faceted, crystallographic features seen in the low ΔK crack growth region of the control samples are seen in the hot cracked samples. This implies the crack growth mechanisms for both types of cracks are identical.

Reflected Light Microscopy

The crack propagation paths for both the hot crack and control samples were studied with RLM to determine if the crack preferred any microstructural feature to propagate through during growth. Figure 6a shows a region of crack growth in a control sample and the crack is obviously growing across the dendrite arms perpendicular to their growth direction. Figure 6b is an area of fatigue crack growth near a hot crack. It is obvious that the crack is not following the interdendritic region as none of the phases present along the initial hot crack are found along the subsequent fatigue crack path. The crack does appear to grow across the secondary dendrite arms identically to that seen in the control samples. This is observed in all the samples regardless of the orientation of the dendrite arms relative to the stress axis.

Discussion

There is a convincing trend when the FCP data and the SEM and RLM results are analyzed together pointing to identical crack growth behavior between hot cracks and typical fatigue cracks. The fracture surfaces of the hot cracked and control samples at similar ΔK values were very similar and points to the conclusion that the crack growth mechanisms for the control and hot cracked samples are the same. Figure 5 are low ΔK regions of a hot cracked and a control sample. Any differences in the crack growth mechanism would appear in the crack surface morphologies. In addition, despite the scatter, the similarities in the crack growth rates for the two types of samples makes it unlikely anything different is happening in the hot cracked samples versus the control samples. Figure 6 show that for both types of cracks the crack growth was normal to the dendrite growth direction.

The scatter in the FCP data is primarily due to the variation in the dendrite orientation along the crack paths in the samples which minimizes its effect on the conclusions. Figure 6a shows the fatigue crack path in a control sample and the crack path is nearly always normal to the dendrite arms and the interdendritic regions. Thus, as the crack changes direction ΔK will vary and cause the scatter shown in Figure 4. This behavior has been previously reported for 718 by Holdsworth and Hoffelner. (12) The reason for this behavior is that fatigue cracks grow through a material by taking the path that offers the least resistance while maximizing K. The interdendritic region contains large amounts of Laves which has a plate-like morphology and is non-deformable due to its crystal structure. (13) The crack will prefer to grow through the dendrites since they are γ phase (high Ni content) and fairly soft. The growth perpendicular to the dendrite arms is due to the plain strain conditions at the crack tip and the face-center cubic (FCC) structure of the dendrites. It is generally believed that the fatigue process is caused by cumulative damage due to slip at the crack tip. (14) The γ dendrites grow in the $\langle 100 \rangle$ direction (15) and have primary slip directions of $\langle 110 \rangle$ on the $\{111\}$ planes (16). If the fatigue crack grows perpendicular to the dendrite growth direction the orientation of the maximum shear stress at the crack tip will generally coincide with that of the primary slip directions in the dendrite. Obviously every dendrite will not be oriented so that the $\langle 100 \rangle$ direction is parallel to the crack tip, but this orientation is overall an easier path for the fatigue crack than any other. A schematic of this process is shown in Figure 7. The crack will grow up and down the $\{111\}$ planes yet macroscopically be growing across the dendrite arms. This explains the crystallographic nature of the fracture surfaces shown in Figure 5.

An additional source of scatter in the samples could be due to the straightening procedure such that a residual stress gradient could be induced in the sample upon loading. Failure to straighten it completely would result in a residual compressive stress on the front surface while over straightening would result in a residual tensile stress. A residual compressive stress would tend to decrease ΔK while a residual tensile stress would increase ΔK relative to its normal value. It is entirely possible that both tensile and compressive residual stresses affected the

results as there are individual hot cracked samples with FCP curves on either side of the control data curves. The data for each control sample showed no difference in the FCP rates between the front and back of the sample.

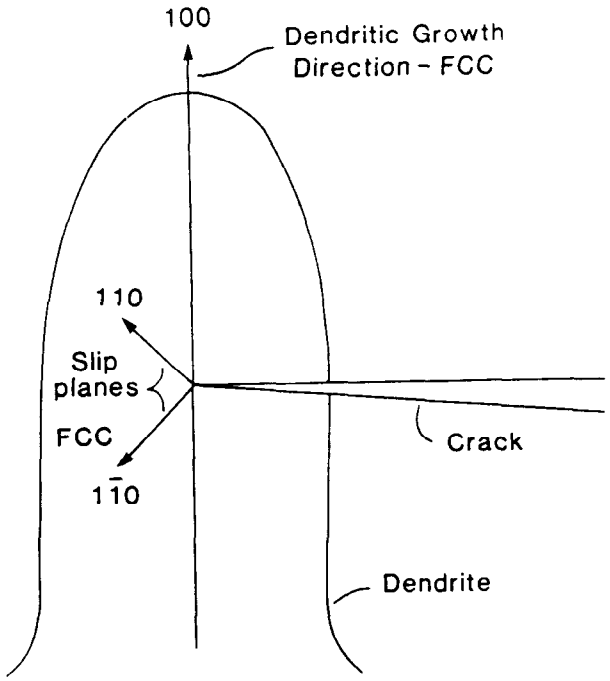

Figure 7 - Diagram of plane strain crack growth through a γ dendrite.

Conclusions

This study set out to determine if welding hot cracks are detrimental to the fatigue behavior of as-cast alloy 718. The hot cracked samples exhibited similar FCP rates to those measured for the control samples tested and the fracture surfaces of both the hot cracked and control samples at similar ΔK values were very similar. The hot cracked samples tested did not exhibit crack growth from the first cycle and apparently the hot cracks require an initiation period before crack growth began. The interdendritic region was found not to influence the FCP rates of either the hot cracked or control samples. In all samples propagation was found to be affected mainly by the orientation of the dendrite arms relative to the crack growth direction.

The data indicates the presence of hot cracks do not adversely affect the fatigue behavior of as-cast alloy 718 any more than the presence of a typical fatigue crack. In fact, hot cracks appear to be less detrimental to the fatigue behavior of alloy 718 than a fatigue crack of identical dimensions due to the probable initiation period required for the hot crack to begin crack growth.

Acknowledgements

The authors would like to thank the Rocketdyne Corp. of Rockwell Intl. for supplying the material used in this study. They would also like to thank Dr. E. L. Bradley, Jr. of the Department of Biostatistics for his help with the regression model. During this work Mr. Bradley was supported by a University of Alabama at Birmingham Graduate School fellowship.

References

1. R. G. Thompson and S. Genculu, "Microstructural Evolution in the HAZ of Inconel 718 and Correlation with the Hot Ductility Test," Welding Journal, 62 (1983), 337s-345s.

2. D. E. Mayo, "Potential Weldability Improvements by Interstitial (C) and Impurity (S) Control in Cast Alloy 718," (Masters' Thesis, University of Alabama at Birmingham, 1987).

3. G. A. Knorowsky, M. J. Cieslak, T.J. Headley, A. D. Romig, and W. F. Hammetter: To be published in Acta Metal.

4. R. G. Thompson, "Microfissuring of Alloy 718 in the Weld Heat-Affected Zone," Journal of Metals, 40(7)(1988), 44-48.

5. L. A. James and W. J. Mills, "Effect of Heat Treatment and Heat-to-Heat Variations in the Fatigue Crack Growth Response of Alloy 718," Eng. Fract. Mech., 22 (1985), 797-816.

6. R. L. Tobler, "Low Temperature Effects on the Fracture Behavior of a Nickel Base Superalloy," Cryogenics, 16 (1976), 669-674.

7. M. Clavel and A. Pineau, "Frequency and Waveform Effects on the Fatigue Crack Growth Behavior of Alloy 718 at 298K and 823K," Metall. Trans., 9A (1979) 471-480.

8. S. Floreen and R. H. Kane, "Effects of Environment on High-Temperature Fatigue Crack Growth in a Superalloy," Metall. Trans., 10A, (1979) 1745-1751.

9. R. G. Thompson et al, "The Relationship Between Grain Size and Microfissuring in Alloy 718," Welding Journal, 64 (1985), 91s-96s.

10. E. L. Bradley, Jr.: Unpublished Results.

11. I. S. Raju and J. C. Newman, Jr., "Stress-Intensity Factors for Two Symmetric Corner Cracks," in Fracture Mechanics, ASTM STP 677, ed. C.W. Smith (Philadelphia: ASTM, 1979), 411-430.

12. S. R. Holdsworth and W. Hoffelner, "Fracture Mechanics and Crack Growth in Fatigue," in High Temperature Alloys for Gas Turbines, ed. R. Burnetaud (Dordrecht: Reidel, 1982), 348-349.

13. C. S. Barrett and T. B. Massalski, Structure of Metals, (Oxford: Pergamon Press, 1980), 256.

14. D. Broek, Elementary Engineering Fracture Mechanics, (Dordrecht: Martinus Nijhoff, 1986), 59-60.

15. M. C. Flemings, Solidification Processing, (New York: McGraw-Hill, 1974).

16. R. W. Hertzberg, Deformation and Fracture Mechanics of Engineering Materials, (New York: John Wiley, 1982), 545.